

ELEVENTH EUROPEAN ROTORCRAFT FORUM

Paper No. 40

DESIGN VERIFICATION AND FLIGHT TESTING OF A BEARINGLESS SOFT INPLANE TAIL ROTOR

B. Enenkl
V. Klöppel

Messerschmitt-Bölkow-Blohm GmbH
Munich, West Germany

September 10–13, 1985
London, England

THE CITY UNIVERSITY, LONDON, EC1V OHB, ENGLAND

DESIGN VERIFICATION AND FLIGHT TESTING OF A BEARINGLESS SOFT INPLANE TAIL ROTOR

B. Enenkl, V. Klöppel
Messerschmitt-Bölkow-Blohm GmbH
Munich, West Germany

Abstract

A composite experimental tail rotor has been developed with the objectives of improved aerodynamic efficiency, gains in simplicity and reduction in weight and cost. To reach these aims a four-bladed bearingless soft inplane rotor was selected. The design uses a fiberglass bending-torsion-flexbeam to accommodate bending deflections and collective pitch control. Theoretical studies are presented dealing with dynamic characteristics, aeromechanic and aeroelastic stability problems, and load and stress aspects.

An extensive ground testing program using a whirl tower with precession capability to generate dynamic loads is described. In addition the ability to simulate ground resonance conditions to test aeromechanic stability was investigated.

Finally, basic ground and flight testing on a BK117 helicopter is presented. These tests were performed to verify ground and air resonance stability and to check the rotor loads as well as the aerodynamic and flightmechanic characteristics.

Notations

$M_{\beta A}$	flap bending moment at $x = 0.037 R$	Ω_{TR}	tail rotor speed (33.8 Hz)
$M_{\zeta A}$	lead-lag bending moment at $x = 0.037 R$	D_δ	collective pitch
M_M	mast moment (140 mm below rotor center)	$\dot{\psi}$	yaw rate
F_{PL}	pitch link load	v	flight speed
R	rotor radius	c_T	equivalent torsional stiffness
x	radius station	δ_δ	pitch-flap coupling
Ω	main rotor speed (6.39 Hz)	D_{NR}	modal damping in the non-rotating system
		ω_ξ	natural inplane frequency
		D_ξ	modal inplane damping (rotating system)

1. Introduction

In the past, several bearingless tail rotors have been developed at Sikorsky, Boeing Vertol, Hughes (ref. 1 to 3). These tail rotors are all of the stiff inplane type. Contrary to this the tail rotor described in this paper is a soft inplane system. The reasons for the development of such a system are the low lead-lag bending moments at the blade root, a torsionally soft flexbeam due to the relatively small edgewise extension of the flexbeam cross section and the avoidance of a potential flap-lag instability. On the other hand the problems of ground and air resonance and of the technical realization of the low lead-lag natural frequency have to be overcome.

The general advantages of bearingless tail rotors are (ref. 4):

- the lower production costs due to greater simplicity
- the reduction of life cycle costs
- the improved reliability mainly due to the fail safe characteristic of these tail rotor systems
- the reduction of weight

The tail rotor described in this paper is an experimental version, which has not been optimized for a particular application. For simplicity the blades are taken from a serial BO105 tail rotor.

The research project has been financed by the German Bundesministerium für Wissenschaft und Forschung.

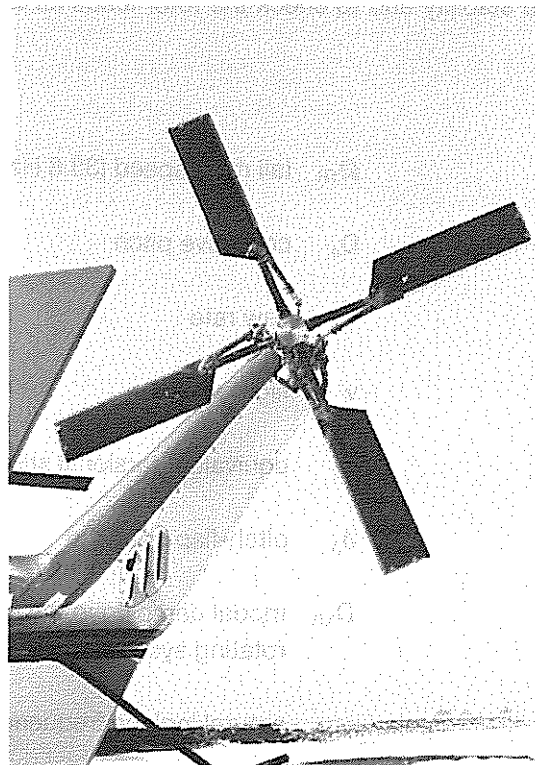


Figure 1 Bearingless Tail Rotor on BK117 Helicopter

2. Description of the Bearingless Rotor System

The structural design is based upon the application of fiber composite materials, eliminating all mechanical elements such as bearings and hinges. A soft fiberglass bending-torsion flexure accommodates bending deflections and collective pitch control. The basic idea of the four-bladed rotor was to use two identical double units with the centrifugal forces of opposing blades being carried directly within the fiberglass straps. Figure 2 shows the structural tailoring of the inboard sections.

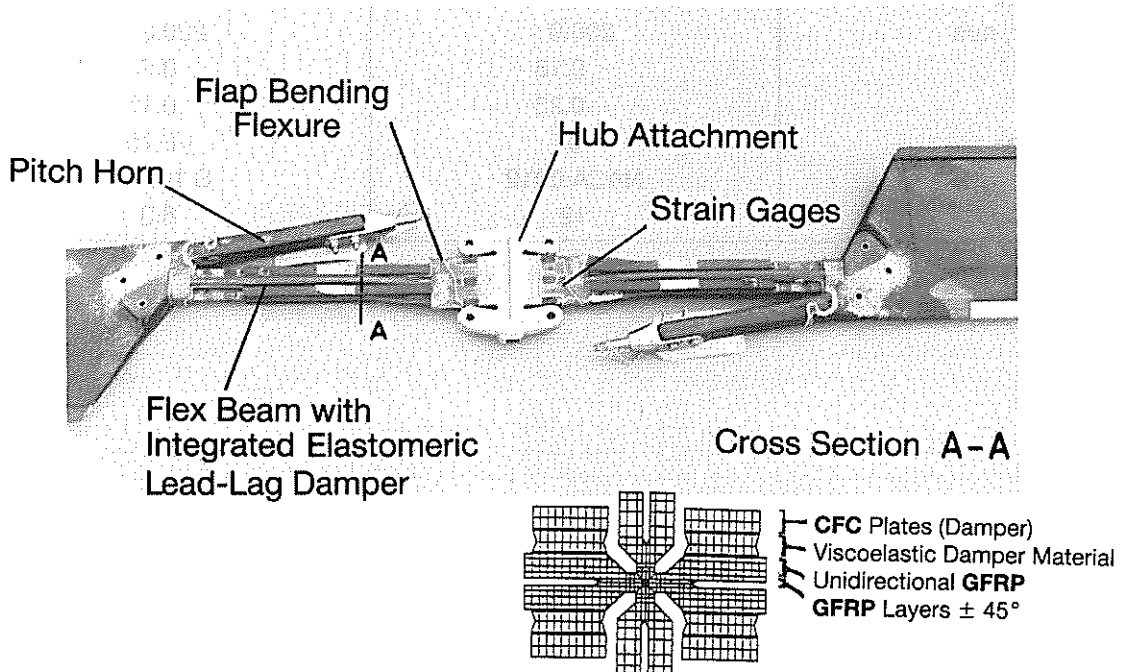


Figure 2 Flexible Element Design

A flat rectangular plate, forming the “flapping hinge”, is continued by the torsional flexure, having a cruciform cross section with an integrated viscoelastic damping element. The pitch-horn is designed in box-beam shape with carbon fiber composite unidirectional straps, providing a high bending stiffness with low mass (ref. 5).

To reduce costs, the experimental rotor was manufactured using untapered and untwisted BO105 standard tail rotor blades with NACA 0012 airfoil. Table 1 compares the basic rotor data of the BK117 A3 production see-saw tail rotor and the four-bladed bearingless tail rotor.

Figure 3 illustrates the structural properties of the experimental rotor blades. The flap bending stiffness distribution is selectively tailored to concentrate flapwise curvature at an inboard radial station, resulting in a low mast moment level. The torsional stiffness of the flexbeam is approximately 5 Nm^2 , leading to a very low equivalent torsional spring of 0.5 Nm/deg . The chordwise bending stiffness distribution illustrates clearly the soft inplane concept of the design.

Table 1 Basic Data

	Bearingless Four-Bladed Experimental Tail Rotor	Production Tail Rotor BK117 A3
Diameter, m	1.95	1.95
Number of Blades	4	2
Rotor Tip Speed, m/s	206.9	220.3
Blade Chord, m	0.18	0.20
Rotor Solidity	0.23	0.13
Linear Twist, deg	0	-6.75
Airfoil	NACA 0012	S 102 E
Thickness, %	12	8.3

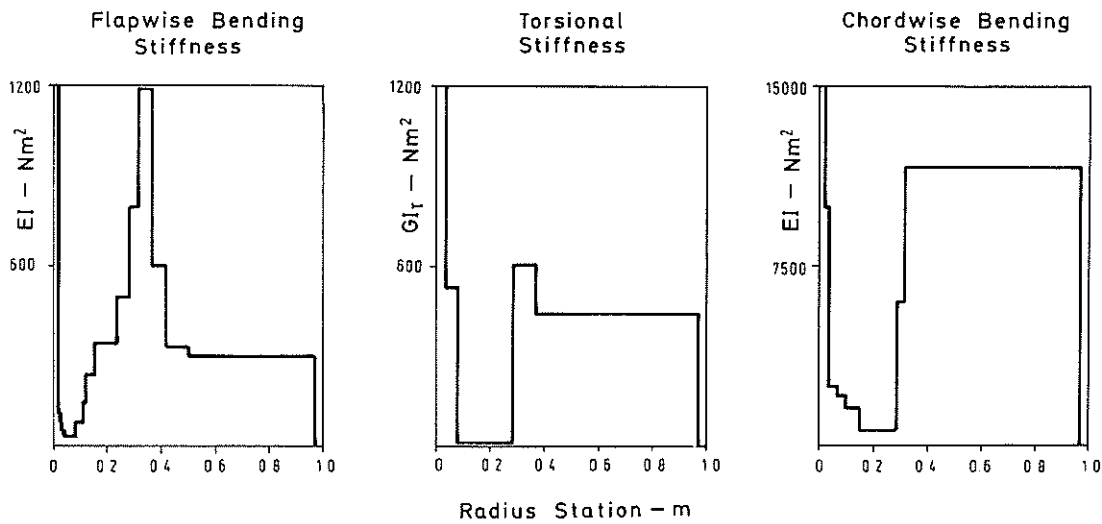


Figure 3 Section Structural Properties

3. Whirl Tower Test

Whirl tower tests were conducted in order to check the rotor system's power/thrust characteristics, dynamic properties and the ability to carry the expected flights loads. During the first run at 100% rpm, the cantilever pitch arm of one blade failed due to inadequate at the root. At the same time, a beginning tendency fo flutter was observed. After this run, the system was modified to strengthen the pitch arm and improve flutter margins. The pitch arm root was reinforced, its length was increased in order to decrease the flap-torsion coupling (δ_3), and the Chinese weights, accomplishing low control forces, were removed. The subsequent whirl tower and flight tests were conducted with this configuration.

3.1 Description of the Test Stand

The test stand is shown in figure 4. It is driven by a 250 kW hydraulic motor and has the ability to rotate up to 20 rpm around its vertical axis in order to excite flap, lag and torsion motions of the tail rotor blades. Stiffness and damping in the vertical plane perpendicular to the rotor axis is adjustable to allow for realistic but controllable simulation of ground resonance conditions. For dynamic excitation in the fixed and rotating systems, electrodynamic and hydraulic shakers were used.

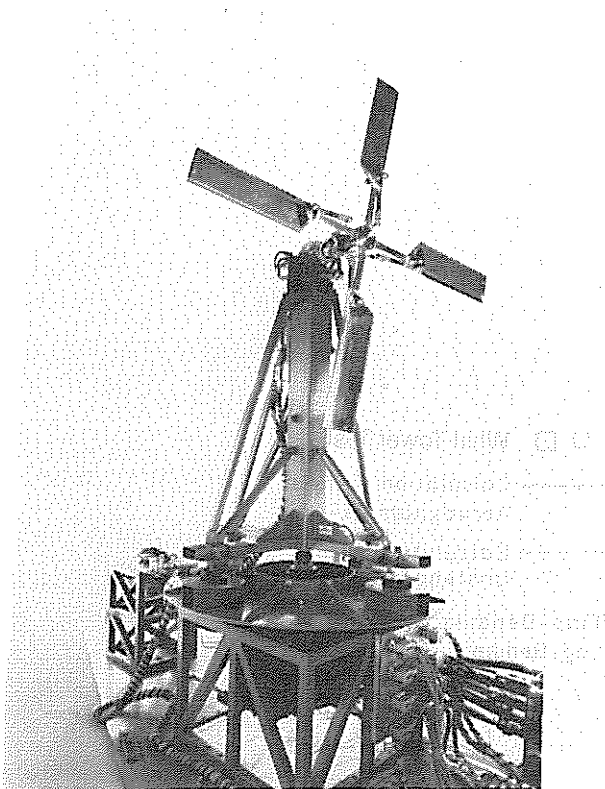


Figure 4 Tail Rotor Whirl Tower at MBB

-
- 250 kW Hydraulic Motor
 - Thrust/Power Characteristics
-
- Precession Capability (120 deg/sec)
 - Cyclic Load Generation
-
- Tuning of Natural Frequency and Damping
 - Ground Resonance Testing
-
- Excitation in the Rotating and Fixed System
 - Measurement of Rotor Natural Frequencies
 - System Damping Analysis
-

3.2 Rotor Dynamics and Aeroelastics

The analysis of the dynamic and aeroelastic characteristics of the experimental rotor system was established by a coupled flap bending/torsion calculation. For the inplane modes an uncoupled computer program was used. The essential results are summarized in table 2.

Table 2 Dynamic Characteristics of the Experimental Tail Rotor

Rotor Speed 100 %, 2026 RPM

Flap Frequency Ratio	1.048
Inplane Frequency Ratio	0.75
Equivalent Hinge Offsets	
Flap, % R	5.5
Lead-Lag, % R	17.5
Lock Number	3.8
Equivalent δ_3 -Angle, deg	+29

Figure 5 shows the natural frequencies of the first inplane mode and the first, second, and third flap bending/torsion modes. The dotted lines indicate the influence of aerodynamics. Test frequencies obtained at zero and up to operating rotor speed are superimposed on the resonance diagram. The excitation of the inplane mode was successful using fixed system excitation of the whirl tower.

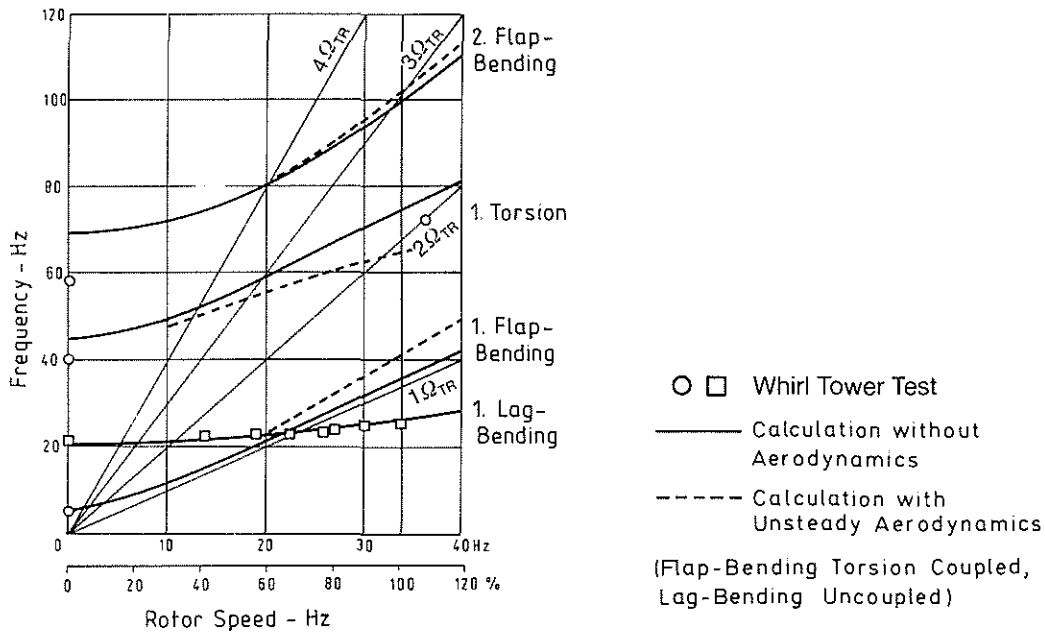


Figure 5 Blade Natural Frequencies

The increase of the first flap bending frequency is caused by the positive δ_3 -coupling (pitch down with flap up) which is derived theoretically in figure 6. For comparison the diagram also shows the original version with the shorter pitch horn assembly. As previously mentioned this version was dropped due to insufficient aeroelastic stability. Figure 7 shows the calculated shape of the critical flutter mode of the blade. Though the natural frequency of this torsion mode is relatively low, freedom of flutter instability throughout the complete rotor speed range was indicated by calculation.

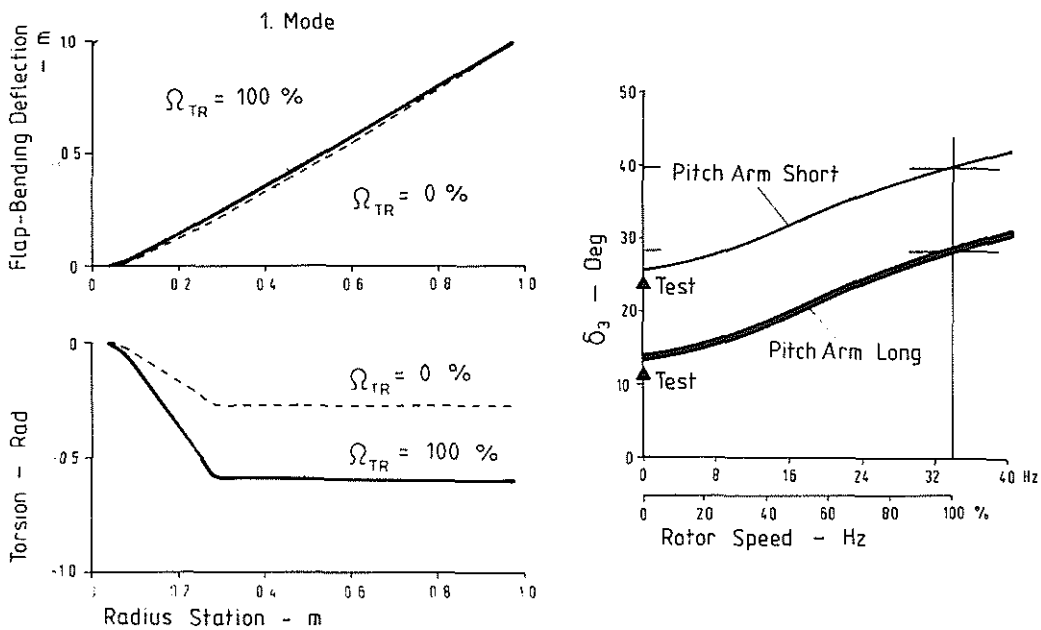


Figure 6 First Flap-Bending-Torsion Mode, δ_3 -Coupling

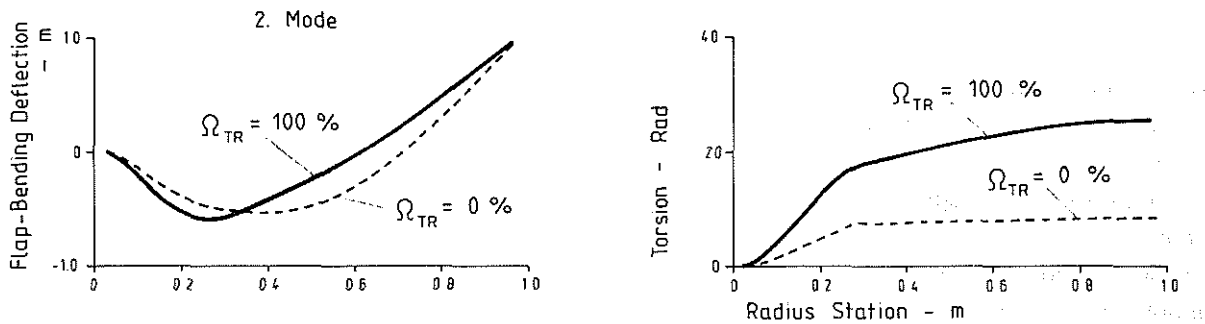


Figure 7 Second Flap-Bending-Torsion Mode, Critical Flutter Mode

3.3 Loads

The most important loads studied during the whirl tower tests were

- the bending moments in the flapping flexure element and
- the control loads.

Due to the removal of the Chinese weights the steady, pitch link loads are significantly higher than those values considered acceptable by pilots in the case of the BO105 and BK117 production tail rotors. On the other hand, the tail rotor described only represents an experimental version whose blade chord would be reduced in the case of any specific application. This would lead to a considerable reduction of the steady pitch link loads due to the lower blade propeller moments (see figure 8). During the flight tests, the experimental tail rotor was controlled by an hydraulic system.

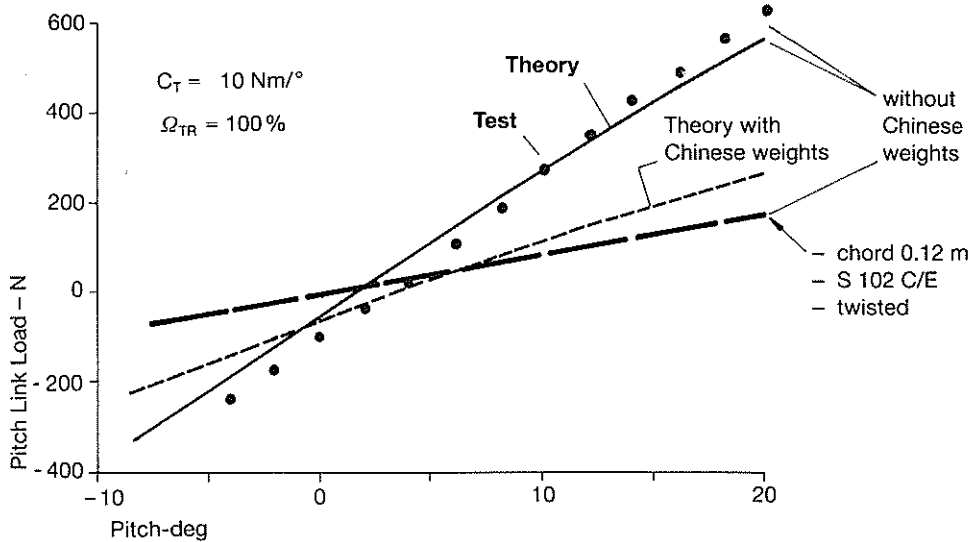


Figure 8 Steady Pitch Link Load

It was found that the most critical design element is the flapping flexure. At nominal rotor speed the tensile strain due to centrifugal force is about 3.6‰. Additional loads caused by steady and vibratory bending moments further increase the strain level.

The precession capability of the whirl tower was used to generate maximum allowable strains. Figure 9 shows the steady and cyclic flapping angles at different pitch settings up to yaw rates of 50 deg/sec. The maximum cyclic loads occur at zero thrust, while the maximum steady loads occur, as expected, at high pitch angles. The diagram indicates a total strain due to flapping of about 3.5‰. This corresponds to a maximum flapping angle of about 2.5 deg. A strain due to inplane bending of about 2‰ (see figure 10) should be added. In total a maximum strain of about 9‰ was measured in the fringe fibers of the rectangular flexure cross section.

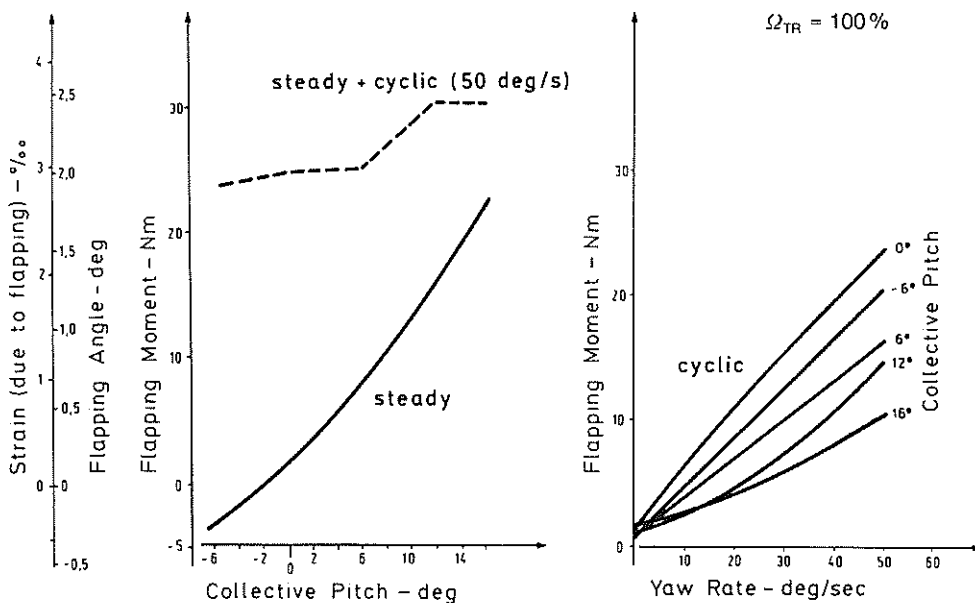


Figure 9 Flap Bending Moment and Flapping Angle during Precession Tests on Whirl Tower (X=0.037 R)

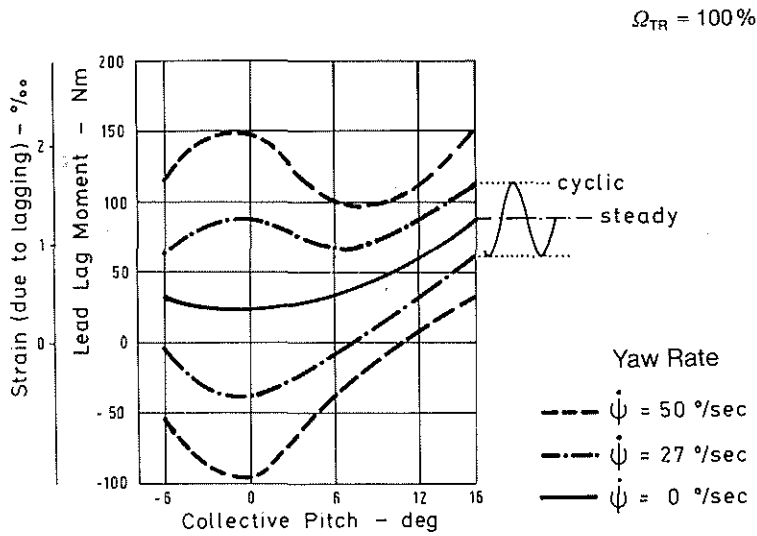


Figure 10 Lead-Lag Bending Moment during Precession Tests on Whirl tower ($X=0.037 R$)

One of the primary design objectives was to keep the equivalent flapping hinge offset low. But from the view-point of strain this is not the optimum design. Figure 11 shows the radial strain distribution in the critical inboard regions due to flapping. There is a maximum at about 0.03 m radial station, which will be avoided in a future optimized design.

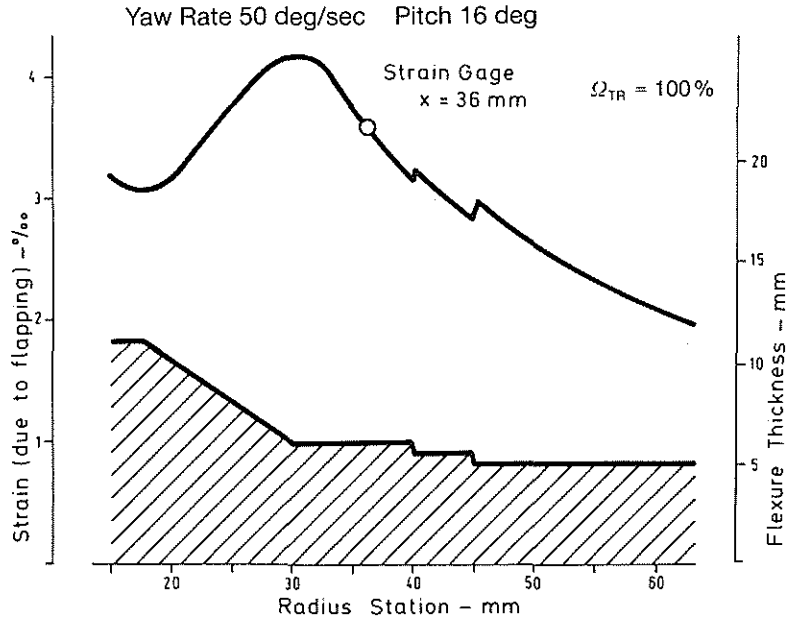


Figure 11 Calculated Strain Distribution Due to Flapping during Precession Tests on Whirl Tower

3.4 Aeromechanical Stability

One of the most critical aspects of the soft inplane concept is the aeromechanical stability of the rotor, ref. 6. Because of this a series of system damping measurements at different whirl tower conditions were conducted. The test stand is designed as a mass-spring-damper system with provisions for tuning the natural frequency and damping in the lateral direction. Figure 12 shows the modal inplane damping in the rotating system of two test stand configurations as a function of collective pitch both experimentally and theoretically, ref. 7. It is to be mentioned that no variation of inplane natural frequency was found in the tested collective pitch range.

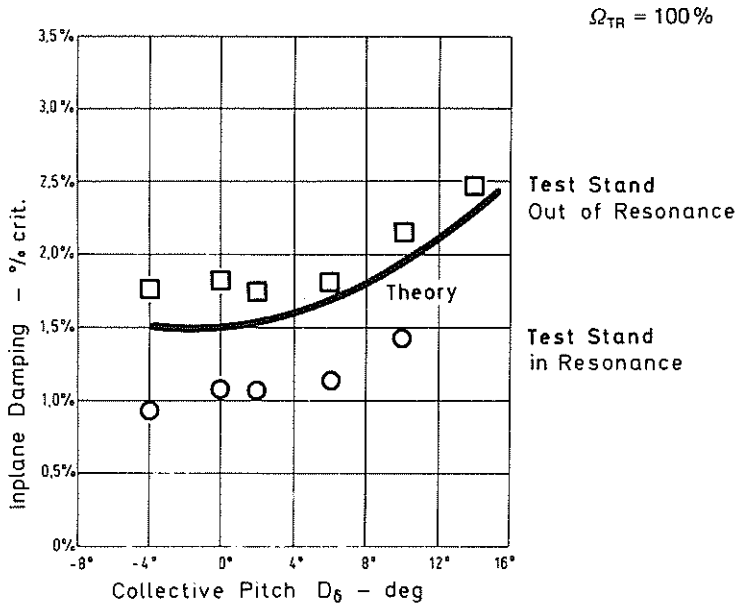


Figure 12 Modal Inplane Damping during Whirl Tower Tests

Damping is measured by the determination of the decay rate of the inplane bending moment after excitation at the resonant frequency. The upper values were obtained with the test stand tuned out of resonance. It is assumed that at low pitch approximately the pure structural damping was measured. The lower test points are the results of a resonance tuning with the regressive inplane mode of the rotor. Figure 13 compares the calculated system damping with tests at 96% and 100% rotor speed. The computation assumes a modal damping of the rotating blade of 1.6% crit. (0 deg pitch) and 2.1% crit. (10 deg pitch), respectively.

As the righthand diagram indicates, the resonance condition occurs slightly below nominal rotor speed. For safety reasons a relatively high test stand damping of about 9% crit. was adjusted. There is good agreement between theory and tests.

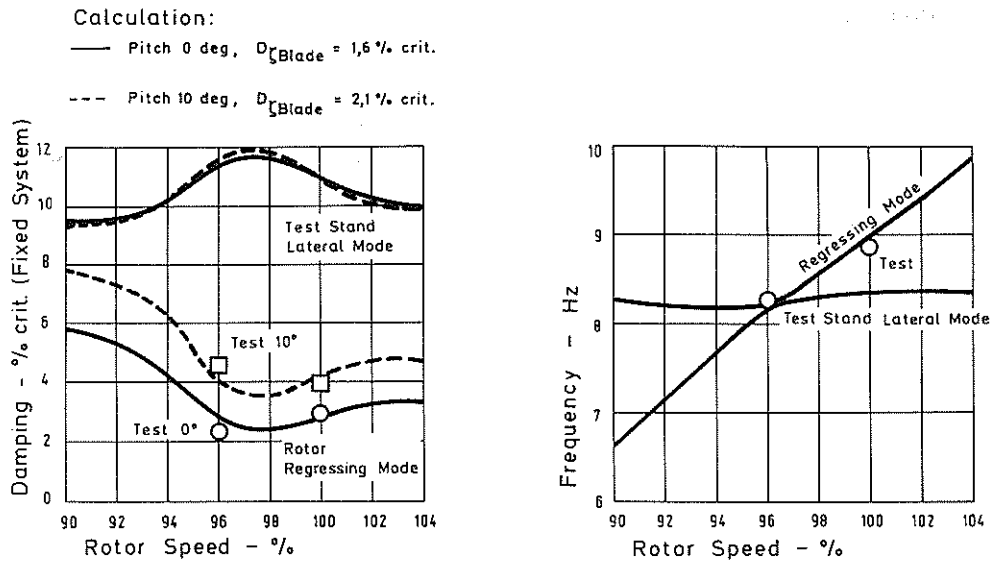


Figure 13 Ground Resonance Stability on Whirl Tower

3.5 Aerodynamics

The thrust/power characteristics of the bearingless tail rotor are shown in figure 14. Due to technical limitations of the test stand control input mechanism, the maximum thrust could not be reached.

Due to the lack of a shear restraint bearing, one part of a defined pitch control input results in a flapping motion of the blade. This leads in connection with the δ_3 -coupling and the blade coning angle at higher thrust to a decrease of the resulting pitch angle.

The required power is expected to be reduced significantly compared to the experimental version by the use of an optimized blade planform and profile.

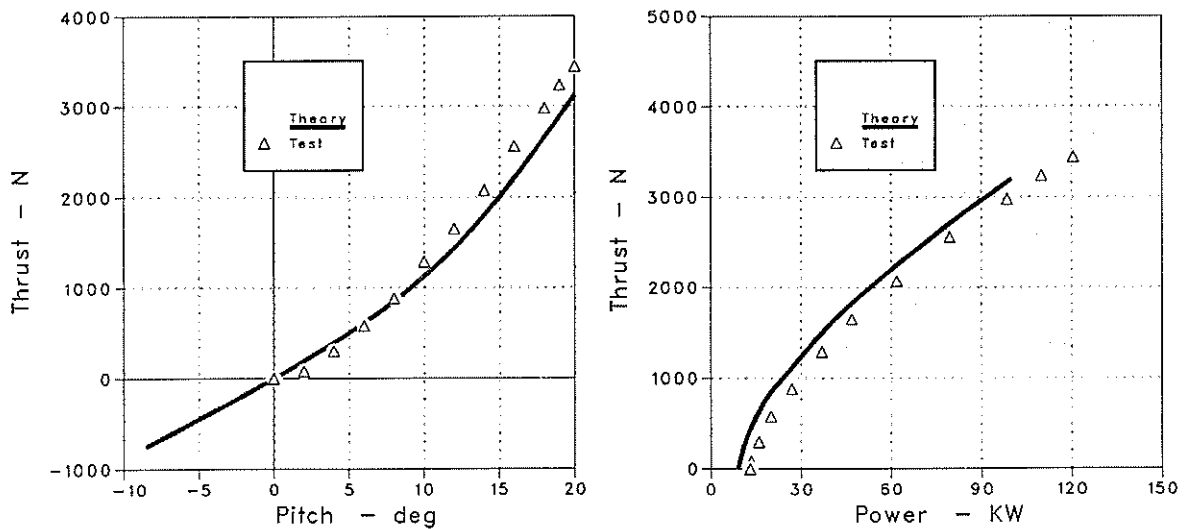


Figure 14 Thrust/Power Characteristics

4. Ground Test on BK117 Helicopter

A potential problem especially for the soft inplane concept is the gravity excitation of the first inplane mode during run-up. The resonance of the first natural lead-lag frequency with 1/rev occurs at 64% of nominal rotor speed (see figure 15). The peak value of the inplane bending moment is not critical because of the lower centrifugal loads. It is even possible to run the tail rotor steadily at resonance conditions.

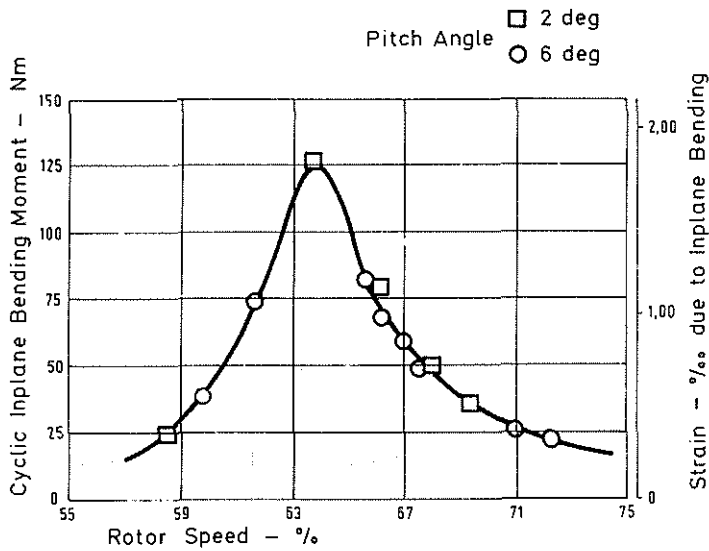


Figure 15 Gravity Resonance Excitation during Rotor Run-Up ($X=0.037 R$)

Figure 16 presents the ground resonance stability calculations on the basis of a finite element analysis of the BK117 airframe. The following fuselage modes contain significant displacements in the vertical plane at the tail rotor hub.

Mode Helicopter on Concrete	Natural Frequency - Hz
F/A Landing Gear	2.7
First Pitch Tailboom	4.4
Pitch Landing Gear	7.9
Pumping Landing Gear	8.9
Yaw Landing Gear	9.9
Flapping Stabilizer	10.4
Second Pitch Tailboom	15.0

Table 3 BK117 Airframe Modes

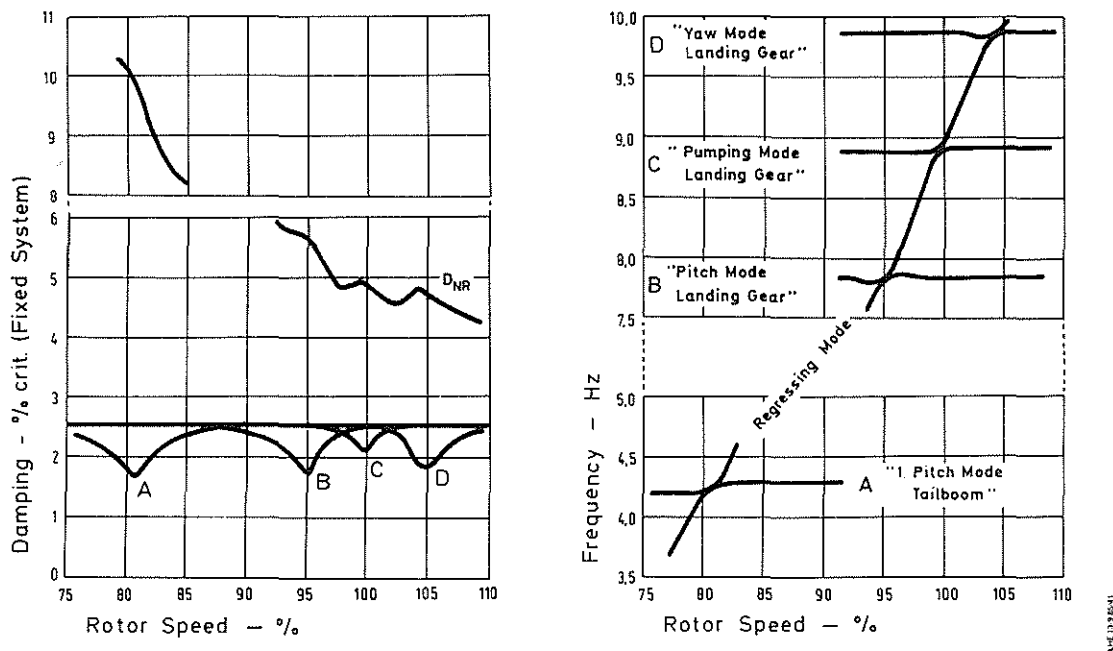


Figure 16 Calculation of Ground Resonance Stability on BK117 Helicopter

The figure illustrates damping and frequency in the fixed system versus rotor speed at zero thrust. The most unfavorable stability condition was expected at the coalescence point of the lead-lag regressing mode with the first tailboom pitch mode (elastic bending mode in the vertical plane). Under the assumption of a structural airframe damping of at least 2.5% and a damping ratio of 1.6% for the rotating blade, the minimum system damping is well above the stability boundary. Although the higher fuselage modes are of less importance, they should not be neglected in the analysis.

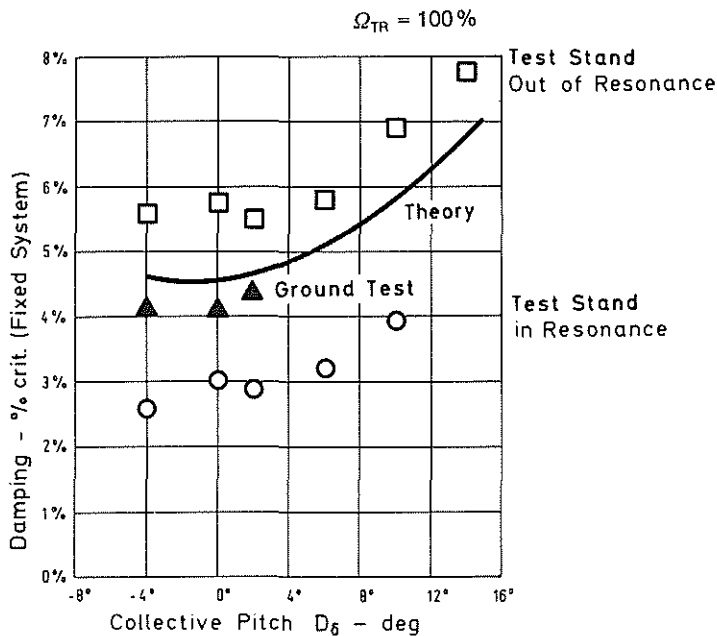


Figure 17 Modal Inplane Damping during Ground Tests

In order to check the system damping on the helicopter, a ground test was conducted before the first flight. An electrodynamic shaker mounted at the tail boom was used to excite the inplane mode of the tail rotor. The main rotor blades were removed to avoid disturbances by the downwash. The landing skids were clamped on the ground. This precaution influences the natural frequency of the first tailboom pitch mode only slightly whereas the landing gear modes increase above the interesting rotor speed range. Figure 17 compares the fixed system damping results with the test stand measurements. The tests were restricted to low pitch settings only.

5. Flight Test

Flight tests were conducted in order to check stress levels, stability and control effectiveness of the bearingless tail rotor. They included

- forward flight up to 132 KIAS
- climbs and descents (MCP, AR) at 60 and 100 KIAS
- turns up to 1.9 g
- sideward flight
- maneuvers to test control potential and flightmechanical stability

5.1 Loads

Blade root flap and lead-lag bending moments, mast moment and pitch link loads were observed with particular interest during the flight tests as these loads are an index for the validity of the tail rotor system. The presentation of the test results concentrates on level flight and descent/climb conditions.

Flap Bending

The flap bending moments at the blade root were the most critical loads, leading to the maximum stresses in the flexbeam area. As expected, the maximum steady flap bending occurred in hover, decreased during moderate forward flight velocities due to the thrust contribution of the vertical tail planes and increased again at higher velocities (see figure 18). The vibratory bending moment shows a similar characteristic with the exception of the hovering condition.

In climb and descent conditions the steady and vibratory blade flap bending moments essentially increase with engine output power, reaching their maxima at MCP. The increase of the vibratory flap bending moments with increasing descent velocity is originated by the tail rotor's negative thrust, necessary to counteract the thrust of the vertical tail planes (see figure 19).

Figure 20 shows the frequency content of the vibratory flap bending moment in level flight. The tail rotor 1/rev is the most significant part of the spectra. Non-harmonic spikes can be identified as main rotor harmonics as they appear in the rotating system of the tail rotor.

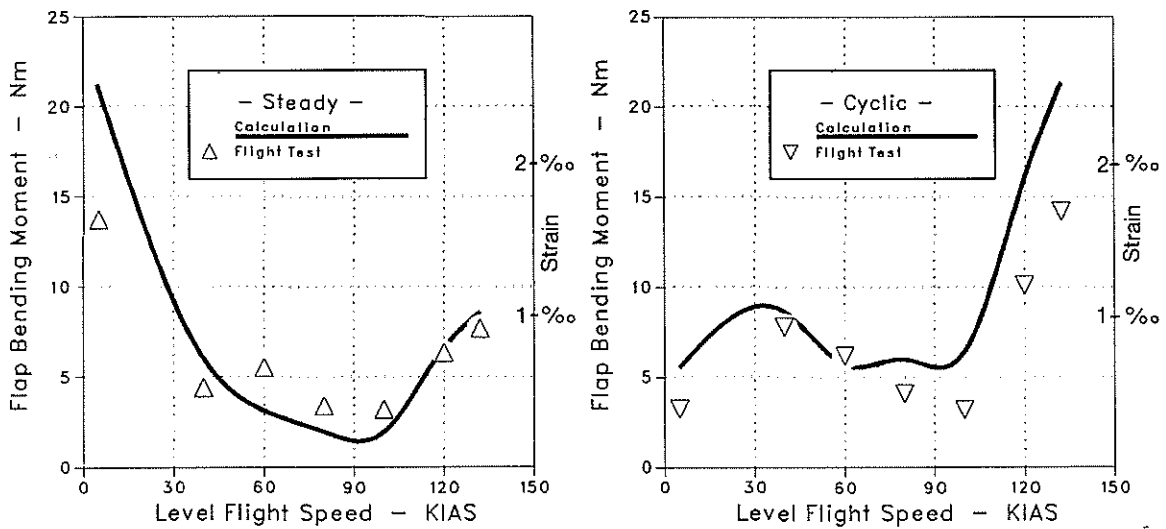


Figure 18 Flap Bending Moment vs Level Flight Speed (x = 0.037 R)

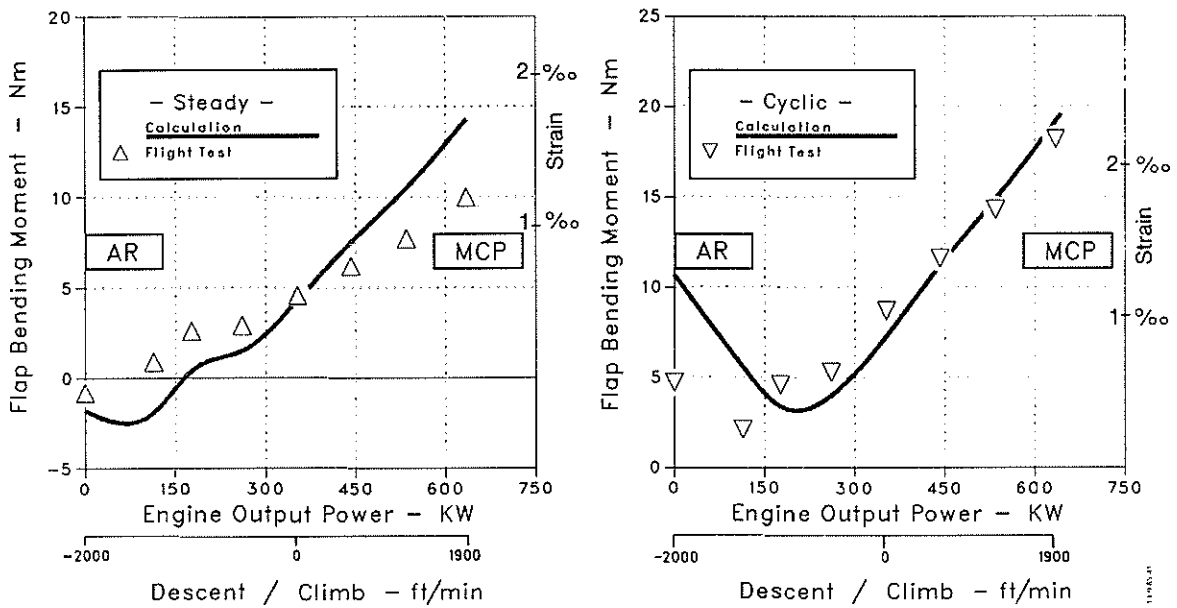


Figure 19 Flap Bending Moment vs Engine Output Power (x = 0.037 R)

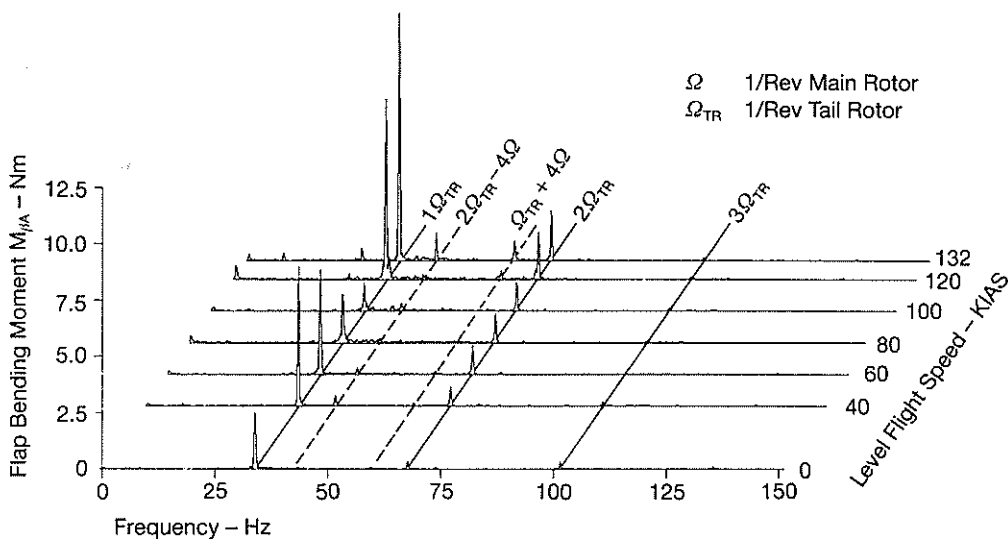


Figure 20 Frequency Spectra of the Flap Bending Moments vs Level Flight Speed ($x = 0.037 R$)

Mast Bending Moment

The mast bending moment follows essentially the vibratory flap bending moment both at forward flight condition and at climbs and descents (see figures 18, 19 and 21).

The moments are as low as in the case of the production see-saw BK117 tail rotor. The frequency spectra are depicted in figure 22.

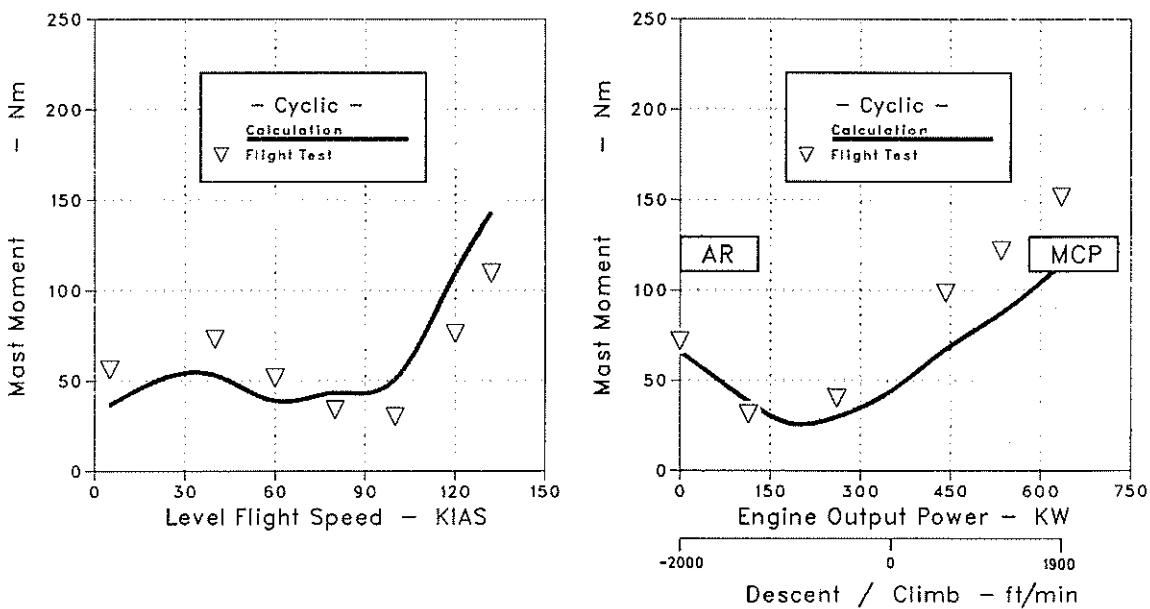


Figure 21 Mast Moment vs Level Flight Speed and Engine Output Power ($v = 60$ KIAS); Measured 140 mm below the Rotor Center

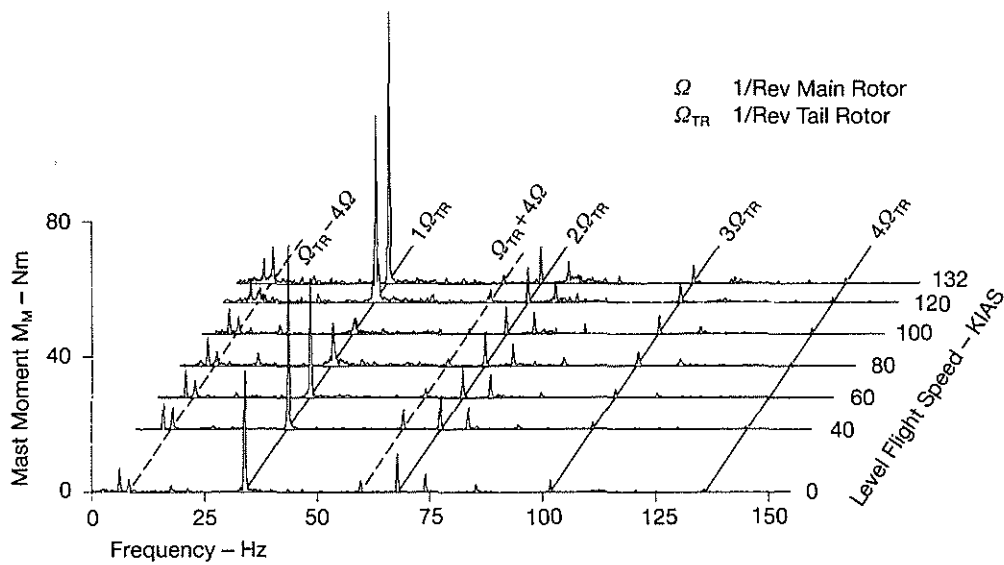


Figure 22 Frequency Spectra of the Mast Moment vs Level Flight Speed

Lead-Lag Bending

A characteristic of the soft inplane bearingless tail rotor is the presence of low dynamic blade lead-lag bending moments. They are shown in figure 23 for level flight conditions and in figure 24 for climbs and descents at a flight speed of 60 KIAS. The steady values correspond to the total required power.

The different steady inplane moments for the 60 KIAS level flight cases in figures 23 and 24 result from different helicopter yaw angles.

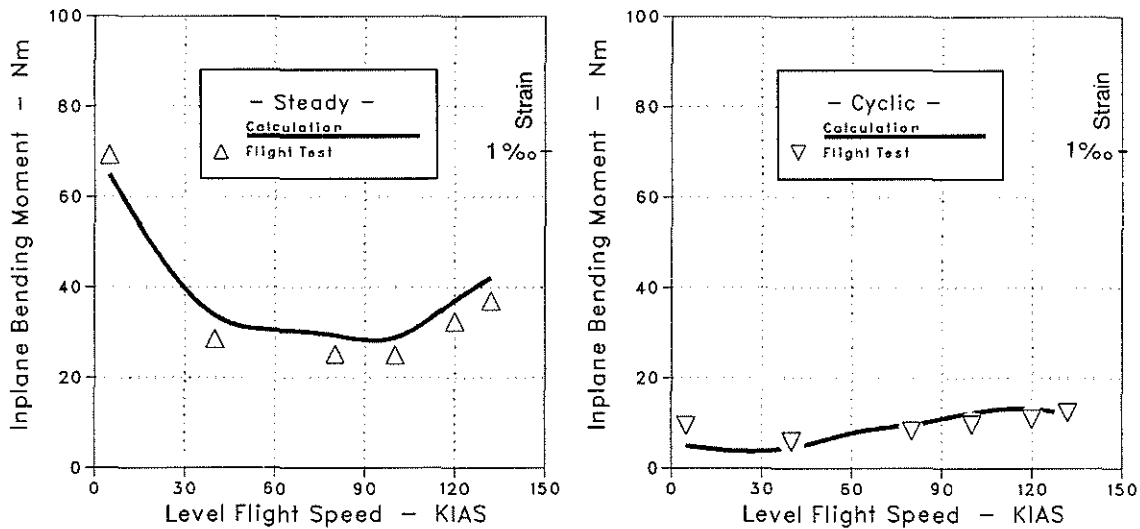


Figure 23 Inplane Bending Moment vs Level Flight Speed ($x = 0.037 R$)

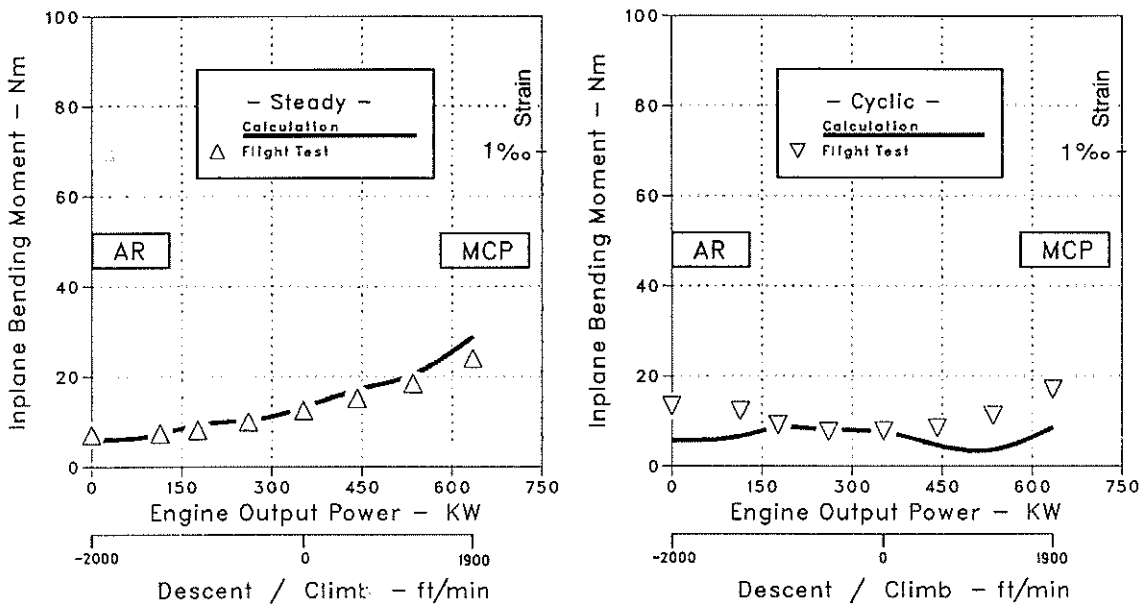


Figure 24 Inplane Bending Moment vs Engine Output Power ($x = 0.037 R$, $v = 60$ KIAS)

The frequency analysis of the measured inplane moment is seen in figures 25 and 26. The 1/rev and 2/rev components have the same order of magnitude. In the frequency range below 1/rev, some transient excitation can be observed. Specifically there are non-harmonic amplitudes which can be identified as the first inplane mode. The amplitude increases with increasing flight speed and with decreasing power setting, respectively.

The flight tests have proved that the inplane damping is sufficient over the whole pitch range.

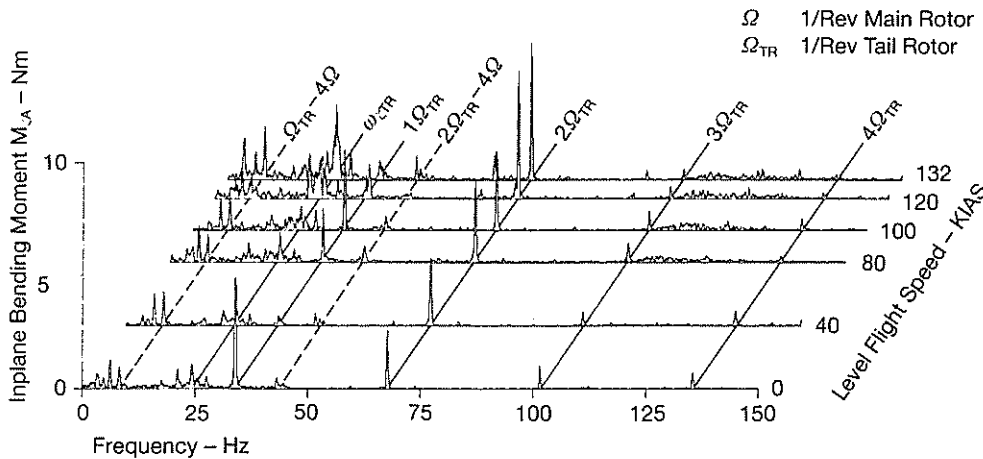


Figure 25 Frequency Spectra of the Inplane Bending Moment vs Level Flight Speed ($x = 0.037 R$)

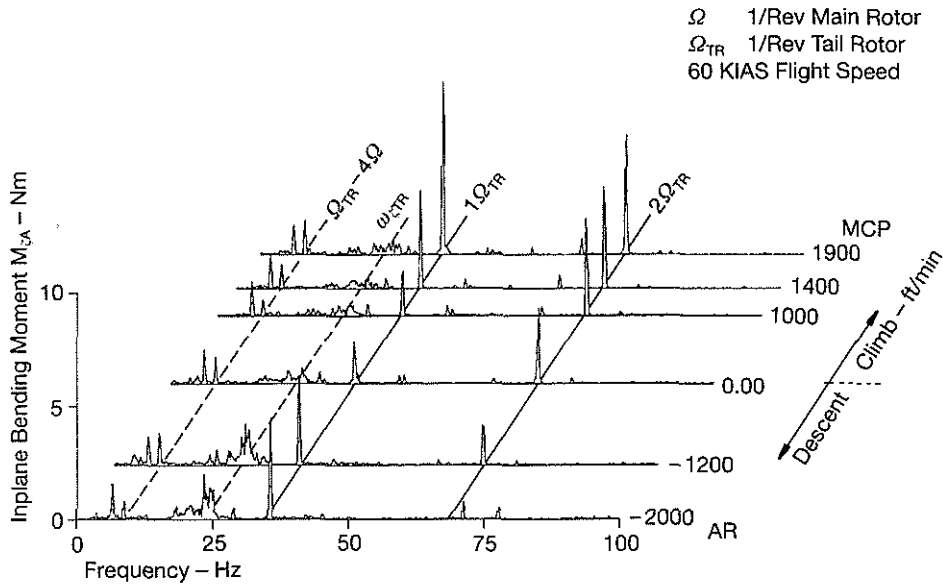


Figure 26 Frequency Spectra of the Inplane Bending Moment vs Descent/Climb Rate ($x = 0.037 R$)

Pitch Link Loads

The steady pitch link loads are primarily a result of the required blade pitch angle as they are dominated by the blade propeller moment. This is recognizable in level flight as well as in climbs and descents (see figures 27 and 28). The vibratory pitch link loads increase at high flight speeds and are mainly determined by the 1/rev and 2/rev components, as seen in the frequency spectra of figure 29. The high 2/rev level is caused by the proximity of the first torsional natural frequency. The 1/rev loads reflect the oscillatory blade torsion moments that are generated by the cyclic flapping and transmitted by the pitch/flap coupling, δ_3 . The level of these blade torsion moments is strongly influenced by the large chord of the experimental tail rotor blades.

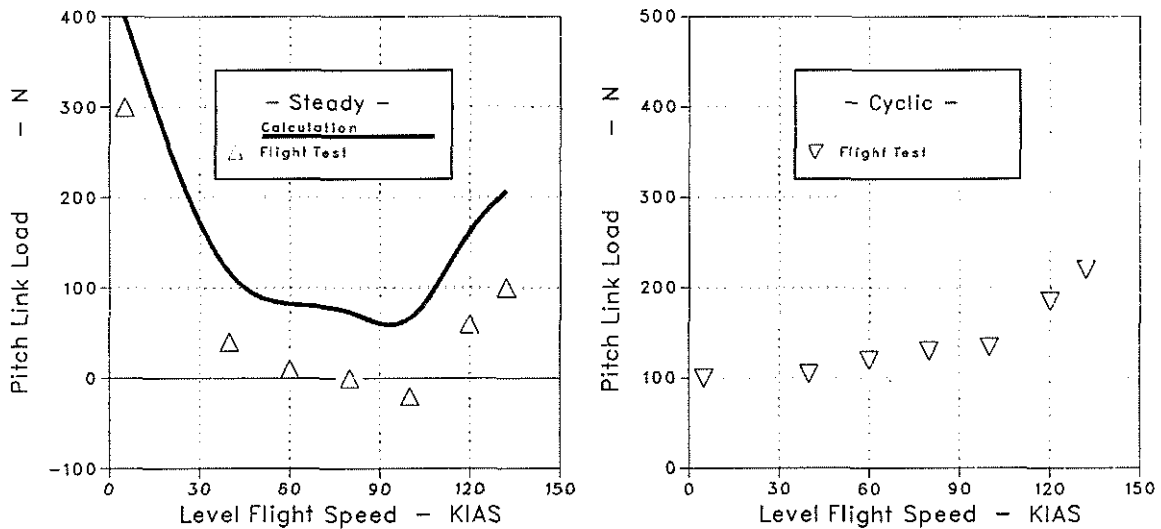


Figure 27 Pitch Link Loads vs Level Flight Speed

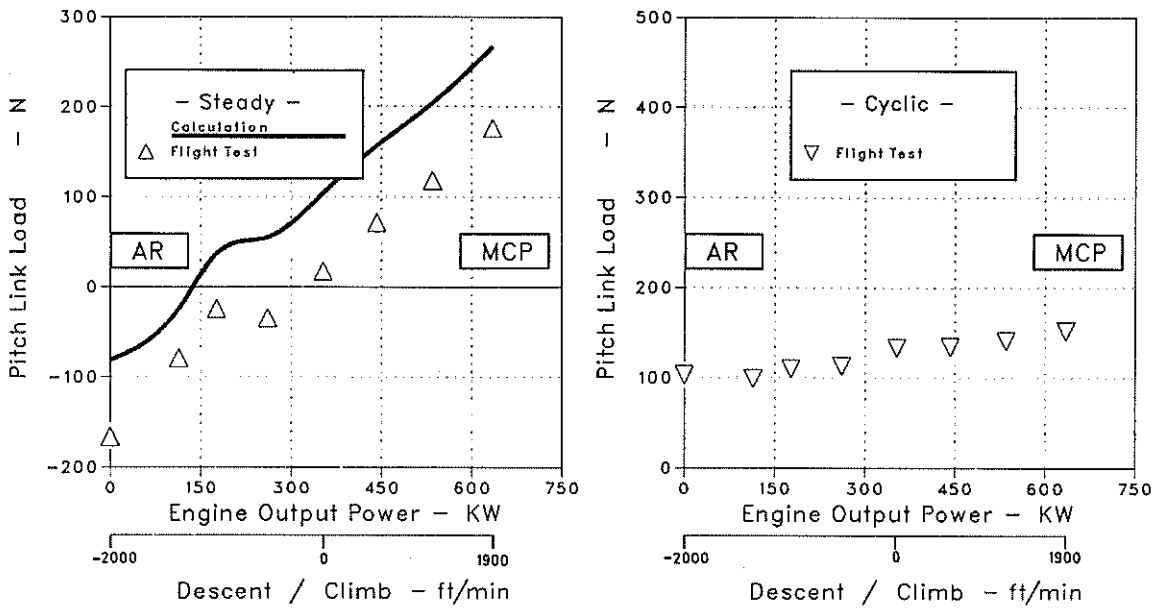


Figure 28. Pitch Link Loads vs Engine Output Power

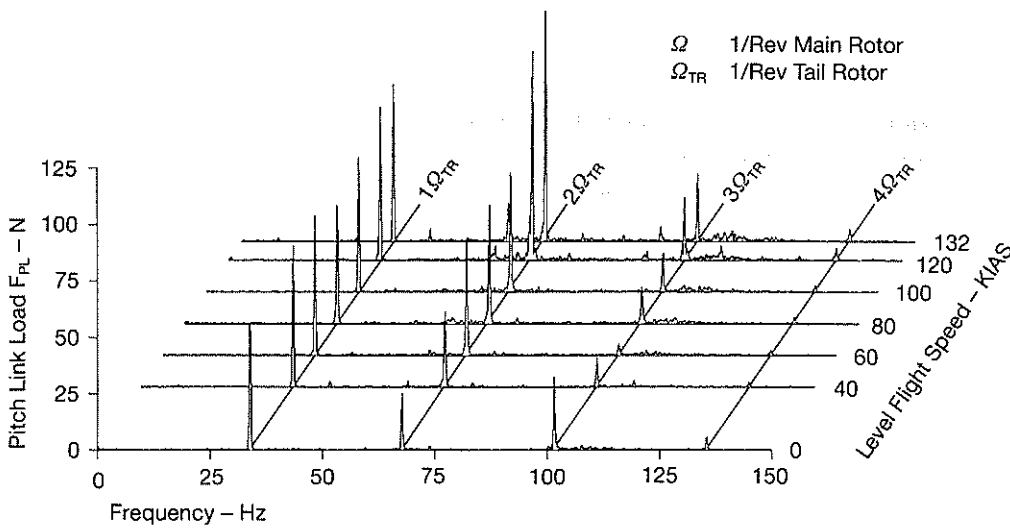


Figure 29 Frequency Spectra of the Pitch Link Load vs Level Flight Speed

Strain Level in the Flapping Flexure

The control potential of the experimental tail rotor was checked by yaw maneuvers. At a maximum yaw rate of about 60 deg/sec the limiting 8‰ strain level in the flapping flexure was reached. As described above combinations of flap and lead-lag bending moments restrict the loading capacity of the flapping flexure. The bending moments in various flight conditions are collected in figure 30. The strain due to the centrifugal force is included in the diagram. It is evident that the flap bending moments are the limiting loads while the inplane loads are relatively low.

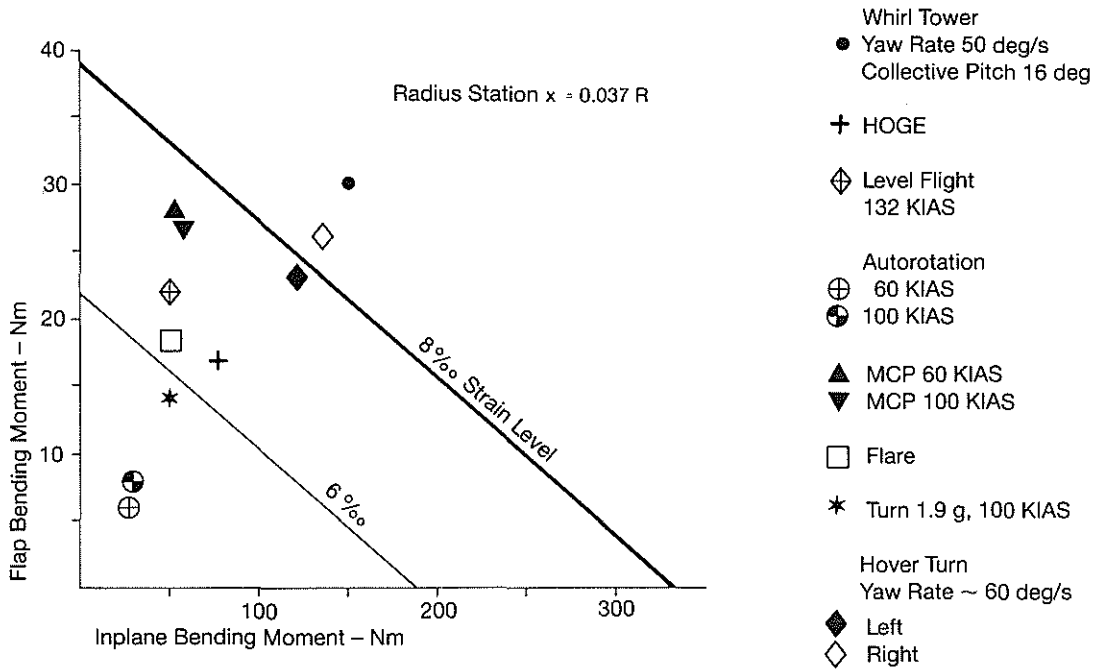


Figure 30 Strain Level in the Flapping Flexure ($x = 0.037 R$)

5.2 Aeromechanical Stability

Theoretical considerations of the aeromechanical stability problem in the air are summarized in figure 31. The resonance diagram on the left shows two airframe modes which cross the regressing inplane frequency in the operational rotor speed range. The two mode shapes of the BK117 fuselage are depicted at the right. The critical one is the tailboom pitch mode. Assuming a structural airframe damping of 2.5% and 1.5% damping of the rotating blades a minimum system damping of about 0.8% was to be expected at 89% rotor speed. This power off condition was not flight tested. The spectral analysis of the flight test data at nominal rotor speed showed no indications of instability problems.

The lead-lag motion could not be excited by impulsive pedal inputs due to the existing inplane damping level. For a measuring of this damping value, a resonant excitation would be necessary.

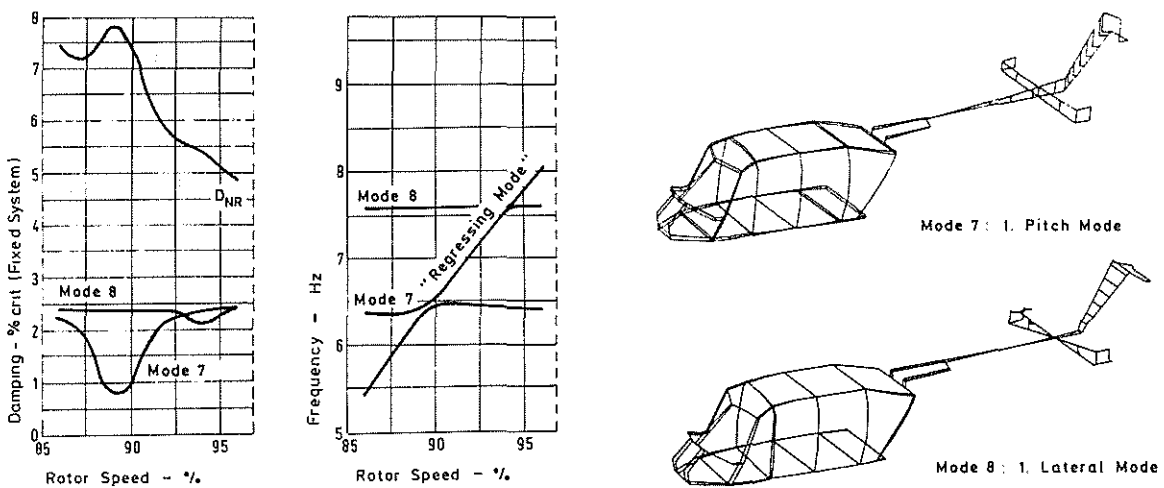


Figure 31 Calculation of Air Resonance Stability on BK117 Helicopter

6. Conclusions

The design verification and the flight testing of the described bearingless experimental tail rotor system was successful.

- An extensive theoretical and experimental investigation of the aeromechanical stability on the BK117 helicopter showed that the soft inplane concept is practicable.
- As expected, the inplane vibratory loads are very low.
- Due to the small equivalent flap hinge offset, the mast moment has the same order of magnitude as in the case of an equivalent see-saw rotor.
- An optimized design of the flapping flexure will limit the strain to an acceptable level at all flight conditions.
- The pitch link loads, controlled by a servo hydraulic system during the test can be reduced by a smaller blade chord.
- The Torsional frequency and the flutter stability margin can be increased by a shear restraint bearing.

It is intended at MBB to continue the development of this bearingless tail rotor system by optimizing the flexural element design and the pitch input mechanism. An advanced blade design will significantly improve the performance.

7. References

- (1) R. R. Fenaughty, N. L. Noehren, Composite Bearingless Tail Rotor for UTTAS, **32nd Annual National V/STOL Forum of the American Helicopter Society, Preprint No. 1084**, May 1976
- (2) J. Shaw, W. T. Edwards, The YUH-61A Tail Rotor: Development of a Stiff Inplane Bearingless Flexstrap Design, **33rd Annual National Forum of the American Helicopter Society, Preprint No. 77. 33-32**
- (3) D. Banerjee, R. A. Johnson, R. H. Messinger, Wind Tunnel Test of a Soft/Stiff Inplane Bearingless Rotor, **Journal of the American Helicopter Society**, April 1984, pp. 52-60
- (4) H. Huber, H. Frommlet, W. Buchs, Development of a Bearingless Helicopter Tail Rotor, **Sixth European Rotorcraft and Powered Lift Aircraft Forum, Bristol, England, Paper No. 16**, September 1980
- (5) G. Seitz, G. Singer, Structural and Dynamic Tailoring of Hingeless/Bearingless Rotors, **Ninth European Rotorcraft and Powered Lift Aircraft Forum, Stresa, Italy, Paper No. 60**, September 1983
- (6) H. Strehlow, B. Enenkl, Aeroelastic Design Considerations in the Development of Helicopters, **56th AGARD Structures and Material Panel Meeting, London**, April 1983
- (7) V. Klöppel, K. Kampa, B. Isselhorst, Aeromechanical Aspects in the Design of Hingeless/Bearingless Rotor Systems, **9th European Rotorcraft and Powered Lift Forum, Stresa, Italy, Paper No. 57**, September 1983